

OBSERVATIONS OF CYANOPOLYINES TOWARD FOUR HIGH-MASS STAR-FORMING REGIONS CONTAINING HOT CORES

KOTOMI TANIGUCHI,^{1,2,*} MASAO SAITO,^{2,1,†} TOMOYA HIROTA,^{3,1} HIROYUKI OZEKI,⁴ YUSUKE MIYAMOTO,²
HIROYUKI KANEKO,² TETSUHIRO MINAMIDANI,^{2,1} TOMOMI SHIMOIKURA,⁵ FUMITAKA NAKAMURA,^{3,1} AND
KAZUHITO DOBASHI⁵

¹*Department of Astronomical Science, School of Physical Science, SOKENDAI (The Graduate University for Advanced Studies), Osawa, Mitaka, Tokyo 181-8588, Japan*

²*Nobeyama Radio Observatory, National Astronomical Observatory of Japan, Minamimaki, Minamisaku, Nagano 384-1305, Japan*

³*National Astronomical Observatory of Japan, Osawa, Mitaka, Tokyo 181-8588, Japan*

⁴*Department of Environmental Science, Faculty of Science, Toho University, Miyama, Funabashi, Chiba 274-8510, Japan*

⁵*Department of Astronomy and Earth Sciences, Tokyo Gakugei University, Nukuikitamachi, Koganei, Tokyo 184-8501, Japan*

(Received; Revised; Accepted)

Submitted to ApJ

ABSTRACT

We carried out line survey observations at the 26–30 GHz band toward the four high-mass star-forming regions containing hot cores, G10.30-0.15, G12.89+0.49, G16.86-2.16, and G28.28-0.36, with the Robert C. Byrd Green Bank Telescope. We have detected HC₅N from all of the sources, and HC₇N from the three sources, except for G10.30-0.15. We further conducted observations of HC₅N at the 42–46 GHz and 82–103 GHz bands toward the three sources, G12.89+0.49, G16.86-2.16, and G28.28-0.36, with the Nobeyama 45 m radio telescope. The rotational lines of HC₅N with the high excitation energies ($E_u/k \sim 63 - 100$ K), which are hardly excited in the cold dark clouds, have been detected from the three sources. The rotational temperatures of HC₅N are found to be $\sim 13 - 20$ K in the three sources. The detection of the lines with the high excitation energies and the derived rotational temperatures indicate that HC₅N exists in the warm gas within 0.07–0.1 pc radii around massive young stellar objects. The column densities of HC₅N in the three sources are derived to be $(\sim 2.0 - 2.8) \times 10^{13}$ cm⁻². We compare the ratios between $N(\text{HC}_5\text{N})$ the column density of HC₅N and $W(\text{CH}_3\text{OH})$ the integrated intensity of the thermal CH₃OH emission line among the three high-mass star-forming regions. We found a possibility of the chemical differentiation in the three high-mass star-forming regions; G28.28-0.36 shows the largest $N(\text{HC}_5\text{N})/W(\text{CH}_3\text{OH})$ ratio of $> 8.0 \times 10^{14}$ in units of (K km s⁻¹)⁻¹ cm⁻², while G12.89+0.49 and G16.86-2.16 show the smaller values ($\sim 2 \times 10^{13}$).

Keywords: astrochemistry — ISM: molecules — stars: formation

Corresponding author: Kotomi Taniguchi
kotomi.taniguchi@nao.ac.jp

* Research Fellow of Japan Society for the Promotion of Science

† The present address : National Astronomical Observatory of Japan, Osawa, Mitaka, Tokyo 181-8588, Japan

1. INTRODUCTION

As the star formation process progresses, the chemical composition of molecular gas changes. The star formation starts with the cold dark molecular clouds ($T \sim 10$ K, $n \sim 10^4$ cm $^{-3}$). In the dark clouds, carbon-chain molecules such as CCS and HC $_5$ N are abundant (Suzuki et al. 1992; Hirota et al. 2009). After formation of protostars, the cloud temperature rises. Such physical changes significantly affect the chemical composition, leading to hot core chemistry in the high-mass star-forming regions and hot corino chemistry in the low-mass star-forming regions. In hot core and hot corino regions ($T \geq 100$ K, $n \sim 10^6$ cm $^{-3}$), while carbon-chain molecules except for HC $_3$ N are deficient, saturated complex organic molecules (COMs) such as CH $_3$ OH and CH $_3$ CN are rich. These COMs are formed by the combination of the grain-surface reactions and the following gas-phase reactions (e.g. Garrod & Herbst 2006; Herbst & van Dishoeck 2009).

Conversely, two low-mass star-forming cores with a variety of carbon-chain molecules have been discovered; L1527 in Taurus (Sakai et al. 2008) and IRAS 15398-3359 in Lupus (Sakai et al. 2009a). The rotational temperatures of carbon-chain molecules in L1527 were derived to be $\sim 12 - 15$ K (Sakai et al. 2009b), which are higher than those in the cold dark clouds. Aikawa et al. (2008) and Hassel et al. (2008) showed that CH $_4$, which is evaporated from grain mantles in the warm regions ($T \sim 20$ K) around the protostar, could form carbon chains in the gas phase. In fact, carbon-chain molecules were found to be enhanced in the warm regions where the temperature becomes higher than 20–30 K (Sakai et al. 2010). Such a chemical mechanism was named warm carbon chain chemistry (WCCC, Sakai et al. 2008).

While there have been many studies about carbon-chain molecules in the low-mass star-forming regions, our knowledge of carbon-chain molecules in the high-mass star-forming regions is still poor. As with the low-mass star-forming cores, understanding chemical mechanisms of carbon-chain molecules in the high-mass star-forming cores is one of the keys to revealing the initial conditions of massive star formation. Cyanoacetylene (HC $_3$ N), the shortest member of cyanopolyynes, is one of the hot core tracers (a dense gas tracer; $n_{\text{H}_2} \sim 10^5 - 10^6$ cm $^{-3}$, Bergin et al. 1996), whereas longer cyanopolyynes are rarely detected. Chapman et al. (2009) demonstrated their chemical model calculation, and suggested that cyanopolyynes (HC $_{2n+1}$ N; $n = 1 - 4$) could be efficiently formed by the neutral-neutral reactions between CN and C $_{2n}$ H $_2$. The latter is formed from C $_2$ H $_2$ evaporated from grain mantles in hot core regions. Taniguchi et al. (2016b) proposed that the main formation pathway of HC $_3$ N in the high-mass star-forming region G28.28-0.36 is the neutral-neutral reaction between C $_2$ H $_2$ and CN, which is the same reaction suggested by Chapman et al. (2009), based on their observations of the ^{13}C isotopic fractionation with the Nobeyama 45 m radio telescope. Motivated by the chemical model calculation of Chapman et al. (2009), Green et al. (2014) conducted survey observations of HC $_5$ N using the $J = 12 - 11$ rotational line toward 79 hot cores with the Tidbinbilla 34 m radio telescope, and detected HC $_5$ N toward 35 sources. They could not derive the excitation temperatures due to the detection of the single rotational line which can be excited even in the cold dark clouds. Thus, the detected emission lines may come from the cold envelopes around the protostars. We still cannot confirm that long cyanopolyynes are formed and exist in hot cores.

In this paper, we carried out observations at the 26–30 GHz band toward four high-mass star-forming regions containing hot cores, G10.30-0.15, G12.89+0.49, G16.86-2.16, and G28.28-0.36, with the Robert C. Byrd Green Bank Telescope (GBT)¹. Two rotational transitions of HC $_5$ N ($J = 10 - 9$ and $11 - 10$) and three transitions of HC $_7$ N ($J = 24 - 23$, $25 - 24$, and $26 - 25$) are in the frequency band. HC $_7$ N has been detected in several star-forming regions (Sakai et al. 2008; Cordiner et al. 2012; Friesen et al. 2013; Feng et al. 2015), which is considered as an indicator of cyanopolyne-rich sources. We also observed the rotational lines of HC $_5$ N at the 42–46 GHz and 82–103 GHz bands toward the three sources, except for G10.30-0.15, with the Nobeyama 45 m radio telescope². Several lines of HC $_5$ N with the high excitation energies ($E_u/k \sim 63 - 100$ K) are in the 82–103 GHz band. Such lines are hardly excited in the cold environments, and the detection of these lines means that HC $_5$ N exists in the warm regions, as discussed later. From the results with the two radio telescopes, we derive the rotational temperatures and the column densities of HC $_5$ N in the three sources using the rotational diagram. We confirm that HC $_5$ N exists in the warm gas in the high-mass star-forming regions from the rotational temperatures. The thermal emission line of CH $_3$ OH, which is one of the hot core tracers and representative COMs, is in the frequency band of the GBT observations. The origin of CH $_3$ OH is considered to be different from that of carbon-chain species. We then investigate the relationship between

¹ The National Radio Astronomy Observatory is a facility of the National Science Foundation operated under cooperative agreement by Associated Universities, Inc.

² The Nobeyama 45 m radio telescope is operated by the Nobeyama Radio Observatory, a branch of the National Astronomical Observatory of Japan.

Table 1. Observing parameters

Frequency (GHz)	Telescope	Beam size ($''$)	η_{mb} (%)	T_{sys} (K)	$\Delta\nu$ (kHz)	T_{rms} (mK)
26–30	GBT	27	77	70–100 (April) 90–120 (July)	66	10–17 (T_{mb})
42–46	Nobeyama	37	71	120–150	122.07	6–14 (T_{A}^*)
82–103	Nobeyama	18 ^a	54 ^a	120–200	244.14	3–6 (T_{A}^*)

^aThe values are at the 86 GHz.

HC₅N and CH₃OH in the three high-mass star-forming regions in Section 4.2.1. We found a possibility of the chemical differentiation among the three sources.

2. OBSERVATIONS

We describe the observational details of each frequency band in this section. Table 1 summarizes the observing parameters of each frequency band.

The observed positions, distances, systemic velocities, and related objects (ultracompact H II regions and outflows) of our four targets are summarized in Table 2. We selected these targets from the list of sources detected in HC₅N (Green et al. 2014) by applying the following three criteria:

1. the source declination is above -21° ,
2. the distance (D) is within 3 kpc, and
3. CH₃CN was detected (Purcell et al. 2006).

The first criterion enables us to observe with the GBT and the Nobeyama 45 m telescope. The second criterion is required for preventing from heavy beam dilution. The last one ensures that target sources contain hot cores. CH₃CN is one of the hot core tracers, and it is always detected in the hot gas (> 100 K, Bisschop et al. 2007). Eight sources in the list meet the three criteria. Since our purpose is to derive the accurate rotational temperatures, we chose three sources among the eight selected sources which show the highest peak intensities of HC₅N (G12.89+0.49, G16.86-2.16, and G28.28-0.36). In order to investigate different conditions, we selected one source which shows the low peak intensity of HC₅N (G10.30-0.15) with the high peak intensities of CH₃CN.

2.1. Observations with the Robert C. Byrd Green Bank Telescope (GBT)

We carried out observations with the Robert C. Byrd Green Bank Telescope (GBT) of the National Radio Astronomy Observatory in 2016 April and July. We used the Ka-band receiver to cover the 26.1–29.7 GHz range, except for 28.7–28.9 GHz. The beam size (HPBW), the aperture efficiency (η_{A}), and the main beam efficiency (η_{mb}) of the Ka-band receiver were approximately $27''$, 67%, and 77%, respectively. The typical system temperatures were from 70 to 100 K in April, and from 90 to 120 K in July, depending on the weather conditions and elevations. We used the VEGAS spectrometer whose bandwidth and frequency resolution were 1080 MHz and 66 kHz, respectively. The frequency resolution of 66 kHz corresponds to the velocity resolution of 0.73 km s^{-1} at 27 GHz. The center frequencies of four spectral windows were set at 26.525, 27.425, 28.325, and 29.275 GHz, respectively.

We employed the position-switching mode. The integration time was 60 seconds per on-source and off-source positions. The observed positions of the four target sources are summarized in Table 2. The off-source positions were set to be $+15'$ away in the declination.

The pointing sources were J1850-0001 at $(\alpha_{2000}, \delta_{2000}) = (18^{\text{h}}50^{\text{m}}31^{\text{s}}17, -00^{\circ}01'55''.1)$ for G28.28-0.36, and J1833-2103 at $(\alpha_{2000}, \delta_{2000}) = (18^{\text{h}}33^{\text{m}}39^{\text{s}}93, -21^{\circ}03'40''.769)$ for the others. We checked the pointing accuracy every 1.5-2 hours, and the pointing error was less than $8''$, depending on the weather conditions. We observed the bright radio

Table 2. Properties of our target sources

Source	R.A. ^a	Decl. ^a	D (kpc)	V_{LSR}^a (km s ⁻¹)	Other Association ^b	
	(J2000)	(J2000)			UCHII ^a	outflow
G10.30-0.15	18 ^h 08 ^m 55 ^s .5	-20°05′58″.0	2.1 ^c	13.0	Y	N ^f
G12.89+0.49	18 ^h 11 ^m 51 ^s .4	-17°31′30″.0	2.50 ^d	33.3	N	Y ^e
G16.86-2.16	18 ^h 29 ^m 24 ^s .4	-15°16′04″.0	1.67 ^e	17.8	N	Y ^e
G28.28-0.36	18 ^h 44 ^m 13 ^s .3	-04°18′03″.0	3.0 ^c	48.9	Y	Y ^f

^aPurcell et al. (2006)

^bThe symbols of "Y" and "N" represent detection and non-detection, respectively. "UCHII" indicates an ultracompact H II region lies within the Mopra beam ($\sim 38''$). The 6.7 GHz methanol masers are associated with all of the four sources.

^cGreen et al. (2014)

^dReid et al. (2014)

^eLi et al. (2016)

^fCyganowski et al. (2008)

continuum source 3C 286 at $(\alpha_{2000}, \delta_{2000}) = (13^{\text{h}}31^{\text{m}}08^{\text{s}}.288, +30^{\circ}30'32''.96)$ in the beginning of every observing session in order to conduct the absolute flux calibration. The intensity calibration error was less than 5%.

2.2. Observations with the Nobeyama 45 m radio telescope

The observations were carried out between 2017 January and March. We observed toward the three sources G12.89+0.49, G16.86-2.16, and G28.28-0.36. The on-source and off-source positions were set at the same ones with the GBT observations. The position-switching mode was employed, and the integration time was 20 seconds per scan.

We used the Z45 receiver (Nakamura et al. 2015) for the 42–46 GHz band observations. The system temperatures of the Z45 receiver were 120–150 K, depending on the weather conditions and elevations. The main beam efficiency (η_{mb}) and the beam size (HPBW) at 43GHz were 71% and $37''$, respectively. The TZ receiver (Nakajima et al. 2013) was used for the 82–103 GHz band observations. The system temperatures were from 120 to 200 K. The main beam efficiency and the beam size at 86 GHz were 54% and $18''$, respectively.

We used the SAM45 FX-type digital correlator (Kamazaki et al. 2012) in frequency settings whose bandwidths and resolutions are 500 MHz and 122.07 kHz for observations of the Z45 receiver, and 1000 MHz and 244.14 kHz for those of the TZ receiver, respectively. The frequency resolutions correspond to the velocity resolution of ~ 0.85 km s⁻¹.

We checked the telescope pointing every 1.5 hr by observing SiO maser line ($J = 1 - 0$) from OH39.7+1.5 at $(\alpha_{2000}, \delta_{2000}) = (18^{\text{h}}56^{\text{m}}03^{\text{s}}.88, +06^{\circ}38'49''.8)$. We used the Z45 receiver for the 42–46 GHz band observations, and the H40 receiver for the 82–103 GHz band observations. The pointing error was less than $3''$.

3. RESULTS AND ANALYSES

3.1. Results

3.1.1. Observational results with the GBT

We conducted data reduction³ using the GBTIDL⁴. The overviews of obtained spectra toward the four sources are shown in Figures 1 and 2. The rms noise levels are 14, 10, 17, and 11 mK in T_{mb} for G10.30-0.15, G12.89+0.49, G16.86-2.16, and G28.28-0.36, respectively. We fitted the spectra with a Gaussian profile and obtained the spectral line parameters, as summarized in Table 3. The lower detection limit is set to be 4σ .

³ We set the velocity units as "lsrk" in the observational scripts, but we wrote the " V_{LSR} " values in the source catalog. We then shifted the frequency so that the emission peaks of HC₃N correspond to its rest frequency, when we made the final spectra.

⁴ <http://gbtidl.nrao.edu>

Two and three rotational lines of HC₅N ($J = 10 - 9$ and $11 - 10$) and HC₇N ($J = 24 - 23$, $25 - 24$, and $26 - 25$) are in the observed frequency range, respectively. All of the observed rotational lines of HC₅N were detected from all of the four sources. We also detected HC₇N from the three sources, except for G10.30-0.15. Detection of HC₇N has been reported in several star-forming regions (Sakai et al. 2008; Cordiner et al. 2012; Friesen et al. 2013; Feng et al. 2015). The detection of HC₇N from the three high-mass star-forming regions suggests that our target cores contain the long cyanopolyynes abundantly.

In addition, several other lines were detected. The hydrogen recombination lines are prominent only in G10.30-0.15, which seems to be caused by a few ultracompact H II (UCH II) regions associated with G10.30-0.15 (Thompson et al. 2006). Although a UCH II region is associated with G28.28-0.36 (Walsh et al. 2003), we did not detect any hydrogen recombination lines in G28.28-0.36. The rotational lines of HC₃N were detected toward all of the four sources. HC₃N is considered as one of the hot core tracers (a dense gas tracer), and it is usually detected in hot core regions, as mentioned in Section 1. The thermal CH₃OH emission lines ($J_K = 4_0 - 3_1 E$) with the low-excitation energy ($E_u/k = 36.3$ K) were detected except for G28.28-0.36, and its lines with high-excitation energies ($E_u/k \sim 120 - 340$ K) were detected only toward G12.89+0.49. Metastable inversion transition lines of NH₃ with very high-excitation energies, i.e., (J, K) = (8, 8) at 26.51898 GHz ($E_u/k \sim 686$ K) and (J, K) = (9, 9) at 27.47794 GHz ($E_u/k \sim 852$ K), were detected toward G12.89+0.49 and G16.86-2.16. The results indicate that extremely hot gas is contained in these regions (Goddi et al. 2011). The H₂CO ($J_{K_a, K_c} = 3_{1,2} - 3_{1,3}$) emission lines were detected toward G12.89+0.49 and G16.86-2.16.

3.1.2. Observational results with the Nobeyama 45 m radio telescope

We conducted data reduction using the Java Newstar, which is an astronomical data analyzing system of Nobeyama data⁵. Figures 3 and 4 show the spectra of HC₅N at the 42–46 GHz and 82–103 GHz bands, respectively. The rms noise levels are from 6 to 14 mK in T_A^* at the 42–46 GHz band and from 3 to 6 mK at the 82–103 GHz band. Table 4 summarizes the line parameters obtained from the Gaussian fitting. The main beam efficiencies which we used in the analysis are summarized in Table 4.

The signal-to-noise ratios were between 4 and 23. The two rotational lines of HC₅N at the 42–46 GHz band ($J = 16 - 15$ and $17 - 16$) were detected from all of the three sources. Moreover, we detected six rotational lines of HC₅N with the high excitation energies ($E_u/k \sim 63 - 100$ K) from all of the sources. The V_{LSR} values of the detected lines are summarized in Table 4. The V_{LSR} values of the HC₅N lines are consistent with the systemic velocities of each source (Table 2).

3.2. Analyses

We derived the rotational temperatures and column densities of HC₅N in the three sources (G12.89+0.49, G16.86-2.16, and G28.28-0.36) from the rotational diagram analysis, using the following formula (Goldsmith & Langer 1999);

$$\ln \frac{3k \int T_{\text{mb}} dv}{8\pi^3 \nu S \mu^2} = \ln \frac{N}{Q(T_{\text{rot}})} - \frac{E_u}{kT_{\text{rot}}}, \quad (1)$$

where k is the Boltzmann constant, S is the line strength, μ is the permanent electric dipole moment, N is the column density, and $Q(T_{\text{rot}})$ is the partition function. We used 4.330 D (Alexander et al. 1976) for μ of HC₅N. Figure 5 shows the fitting results of the rotational diagram for the three sources. The errors include the Gaussian fitting errors, the uncertainties from the main beam efficiency of 10%, the chopper-wheel method of 10%, and from the other factors such as calibration and filling factor of 30%. Since we do not know the spatial distributions of HC₅N, we assume the filling factor of unity. In the fitting, the values of the $J = 16 - 15$ and $17 - 16$ transitions are systematically lower than the fitting lines. This suggests a smaller filling factor than unity, because the beam size at the 42–46 GHz band with the Nobeyama 45 m telescope is significantly larger than those at the 26–30 GHz band with the GBT and at the 82–103 GHz band with the Nobeyama 45 m telescope. The ranges of the derived rotational temperatures and column densities in the three sources are 17–23 K and $(7.5 - 11) \times 10^{12} \text{ cm}^{-2}$, as summarized in Table 5. In the case of G10.30-0.15, we detected only two lines with the similar energies using the GBT, and we cannot conduct the rotational diagram analysis. We derived the column density of HC₅N in G10.30-0.15 to be $8.5_{-1.7}^{+2.0} \times 10^{12} \text{ cm}^{-2}$, using the average value of the rotational temperatures in the three sources (21 ± 11 K). The error of the rotational temperature in G10.30-0.15

⁵ <http://www.nro.nao.ac.jp/jnewstar/html/>

Table 3. Spectral line parameters observed with the GBT

Species (Transition)	Frequency ^a (GHz)	E_u/k (K)	G10.30-0.15			G12.89+0.49			G16.86-2.16			G28.28-0.36		
			T_{mb} (K)	FWHM (km s ⁻¹)	$\int T_{\text{mb}} dv$ (K km s ⁻¹)	T_{mb} (K)	FWHM (km s ⁻¹)	$\int T_{\text{mb}} dv$ (K km s ⁻¹)	T_{mb} (K)	FWHM (km s ⁻¹)	$\int T_{\text{mb}} dv$ (K km s ⁻¹)	T_{mb} (K)	FWHM (km s ⁻¹)	$\int T_{\text{mb}} dv$ (K km s ⁻¹)
HC ₃ N ($J = 3 - 2$)	27.29429	2.6	1.14 (5)	7.9 (4)	9.6 (6)	1.60 (11)	4.5 (4)	7.7 (8)	1.94 (5)	4.42 (14)	9.1 (4)	2.24 (11)	2.38 (14)	5.7 (4)
HC ₅ N ($J = 10 - 9$)	26.62654	7.0	0.107 (14)	2.9 (4)	0.33 (7)	0.209 (13)	3.5 (3)	0.78 (8)	0.37 (2)	2.6 (2)	1.03 (11)	0.37 (3)	2.08 (17)	0.81 (9)
($J = 11 - 10$)	29.28915	8.4	0.158 (11)	4.7 (4)	0.79 (8)	0.283 (16)	3.6 (2)	1.10 (9)	0.42 (3)	3.1 (3)	1.41 (16)	0.53 (2)	1.91 (9)	1.08 (7)
HC ₇ N ($J = 24 - 23$)	27.07181	16.2	< 0.042	0.076 (8)	4.5 (5)	0.36 (6)	< 0.051	0.086 (10)	2.4 (3)	0.22 (4)
($J = 25 - 24$)	28.19981	17.6	< 0.042	0.051 (8)	3.1 (6)	0.16 (4)	< 0.051	0.083 (12)	2.0 (3)	0.17 (4)
($J = 26 - 25$)	29.32777	19.0	< 0.042	< 0.030	0.104 (12)	1.17 (15)	0.13 (2)	0.098 (12)	1.8 (2)	0.19 (3)
CH ₃ OH ($J_K = 4_0 - 3_1 E$)	28.31607	36.3	0.186 (5)	7.5 (4)	1.48 (10)	0.259 (14)	4.5 (3)	1.25 (10)	0.180 (14)	5.5 (5)	1.06 (13)	< 0.033
SO ₂ ($J_{K_a, K_c} = 4_{0,4} - 3_{1,3}$)	29.32133	9.2	-	-	-	0.16 (4)	5.1 (1.3)	0.9 (3)	0.27 (3)	4.8 (7)	1.4 (2)	0.084 (12)	2.6 (4)	0.23 (5)
H ₂ CO ($J_{K_a, K_c} = 3_{1,2} - 3_{1,3}$)	28.97480	33.4	< 0.042	0.284 (14)	4.5 (3)	1.37 (10)	0.285 (19)	3.5 (3)	1.05 (10)	< 0.033

NOTE—Numbers in the parentheses are the standard deviation of the Gaussian fit, expressed in units of the last significant digits. For example, 1.14 (5) means 1.14 ± 0.05 . We cannot fit the line of SO₂ line for G10.30-0.15 well, as denoted by ‘-’ marks. The upper limits correspond to the 3σ limits.

^a Taken from the Cologne Database for Molecular Spectroscopy (CDMS) (Müller et al. 2005).

Table 4. Spectral line parameters of HC₅N observed with the Nobeyama 45 m telescope

Transition ($J' - J''$)	Frequency ^a (GHz)	E_u/k (K)	G12.89+0.49				G16.86-2.16				G28.28-0.36				η_B (%)
			T_{mb} (K)	FWHM (km s ⁻¹)	$\int T_{mb} dv$ (K km s ⁻¹)	V_{LSR}^b (km s ⁻¹)	T_{mb} (K)	FWHM (km s ⁻¹)	$\int T_{mb} dv$ (K km s ⁻¹)	V_{LSR}^b (km s ⁻¹)	T_{mb} (K)	FWHM (km s ⁻¹)	$\int T_{mb} dv$ (K km s ⁻¹)	V_{LSR}^b (km s ⁻¹)	
16–15	42.60215	17.4	0.186 (7)	3.36 (14)	0.67 (4)	32.7	0.296 (17)	2.69 (18)	0.85 (7)	19.0	0.251 (14)	1.97 (12)	0.53 (4)	49.6	71
17–16	45.26472	19.6	0.148 (8)	3.5 (2)	0.56 (5)	32.4	0.253 (17)	2.8 (2)	0.75 (8)	19.0	0.239 (13)	1.88 (11)	0.48 (4)	49.1	71
31–30	82.53904	63.4	0.096 (7)	3.8 (3)	0.39 (4)	33.6	0.063 (6)	4.0 (5)	0.27 (4)	17.8	0.068 (6)	2.2 (2)	0.16 (2)	49.5	56
32–31	85.20134	67.5	0.092 (8)	3.4 (3)	0.34 (4)	33.7	0.084 (8)	2.8 (3)	0.25 (3)	17.4	0.053 (4)	2.6 (2)	0.144 (17)	49.3	54
34–33	90.52589	76.0	0.109 (7)	4.4 (3)	0.50 (5)	33.3	0.133 (7)	3.1 (2)	0.44 (4)	17.1	0.036 (5)	2.5 (4)	0.10 (2)	49.5	52
36–35	95.85034	85.1	0.063 (5)	4.0 (3)	0.27 (3)	34.1	0.042 (6)	4.4 (7)	0.20 (4)	17.5	0.031 (4)	2.8 (5)	0.09 (2)	49.1	49
38–37	101.17468	94.7	0.034 (4)	6.5 (9)	0.23 (4)	32.3	0.106 (9)	2.9 (3)	0.33 (4)	17.7	0.018 (5)	2.1 (6)	0.039 (16)	49.0	46
39–38	103.83682	99.7	0.035 (5)	4.1 (6)	0.15 (3)	33.0	0.124 (9)	2.7 (2)	0.35 (4)	17.5	0.039 (6)	1.6 (3)	0.069 (17)	49.7	45

NOTE—Numbers in the parentheses are the standard deviation of the Gaussian fit, expressed in units of the last significant digits.

^a Taken from the Cologne Database for Molecular Spectroscopy (CDMS) (Müller et al. 2005).

^b The errors were 0.85 km s⁻¹, which corresponds to the velocity resolution (Section 2.2).

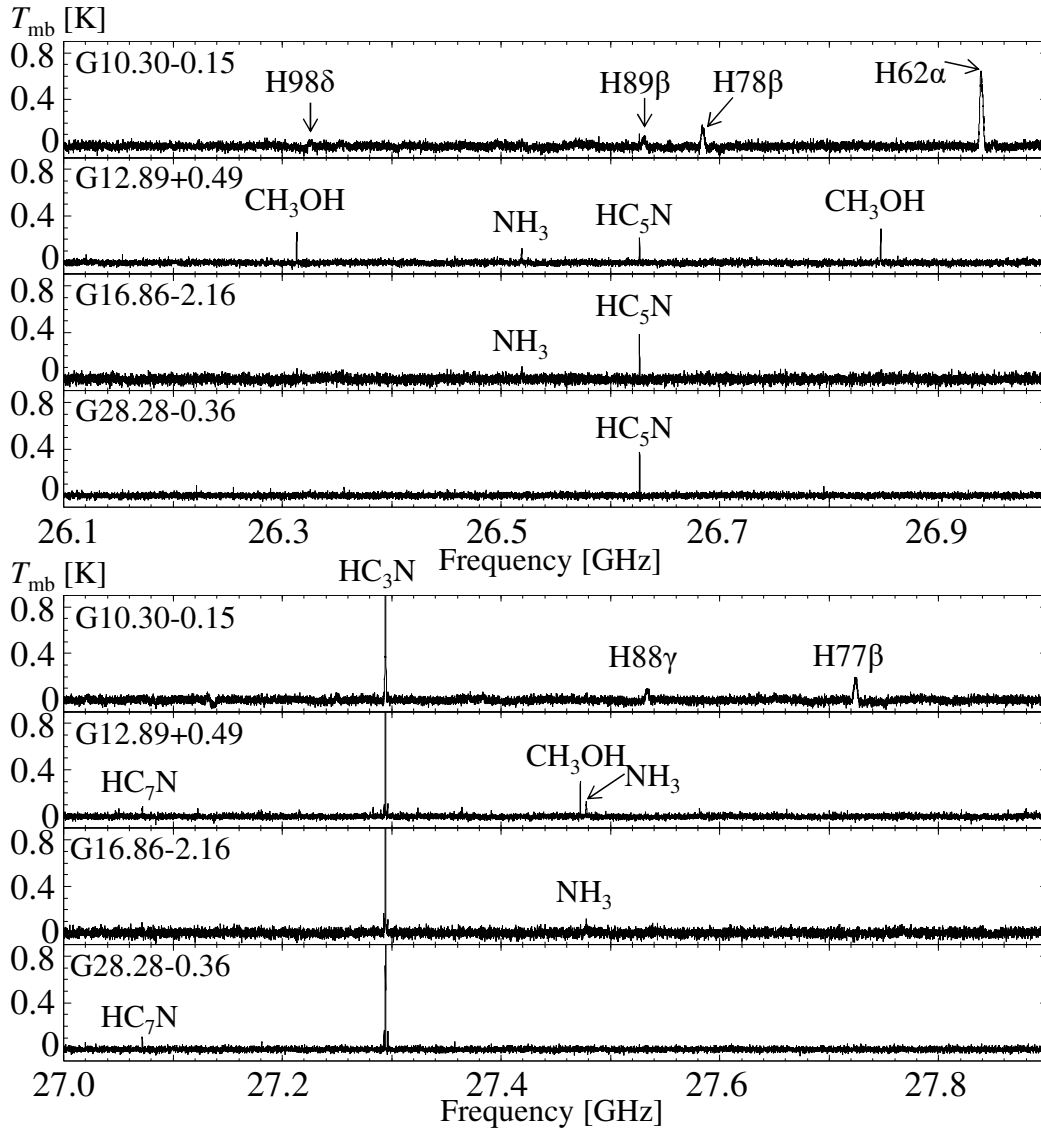


Figure 1. Spectra toward the four hot cores from 26.1 to 27.0 GHz (upper) and from 27.0 to 27.9 GHz (lower) with the GBT. The source names are presented at upper left parts of each panel. The frequency resolution is 66 kHz.

was estimated from the relative errors of the rotational temperatures in the three sources, and the error of the column density corresponds to the change in the rotational temperature.

Assuming a small beam filling factor, we multiplied the integrated intensities of the GBT data by $(\frac{27''}{18''})^2$ and the 45GHz band data by $(\frac{37''}{18''})^2$ for the correction of the different beam sizes. Figure 6 shows the rotational diagram with the beam-size correction. All of the data, including the 42–46 GHz band, are better fitted. From the above

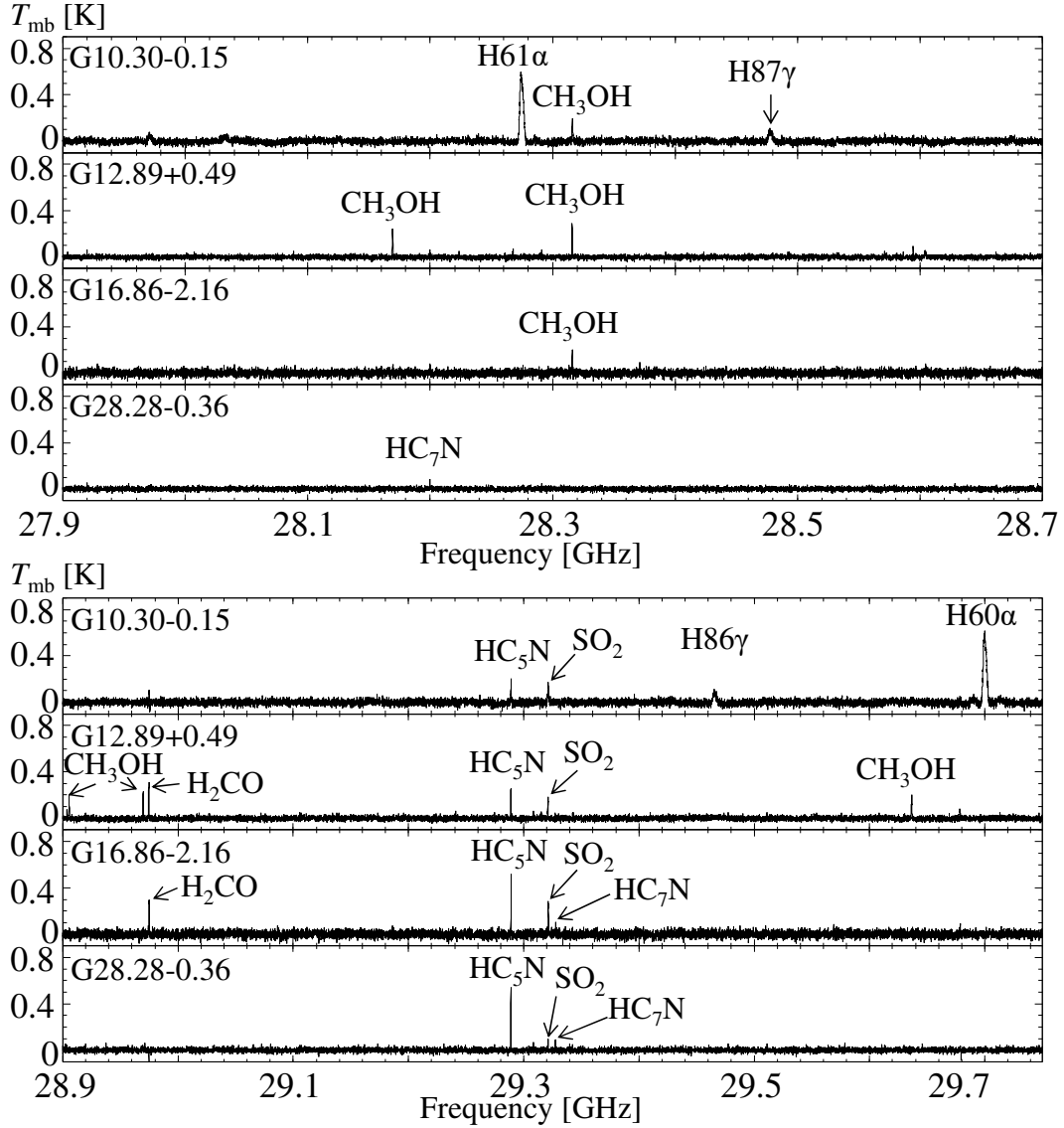


Figure 2. Spectra toward the four hot cores from 27.9 to 28.7 GHz (upper) and from 28.9 to 29.7 GHz (lower) with the GBT. The source names are presented at upper left parts of each panel. The frequency resolution is 66 kHz.

considerations of beam sizes and a small beam filling factor, the emission region sizes are limited to below $18''$, which correspond to $0.07\text{--}0.1$ pc radii at the target source distances (1.67–3.0 kpc, Table 2).

Table 5 summarizes the derived values of the rotational temperatures and column densities. The rotational temperatures are derived to be 13.8–18 K, and the corresponding column densities are $(2.05\text{--}2.78) \times 10^{13} \text{ cm}^{-2}$. The derived rotational temperatures with and without the beam-size correction are consistent within their 1σ errors. The rotational temperature and the column density in G10.30-0.15 were derived by the same manner as mentioned in the

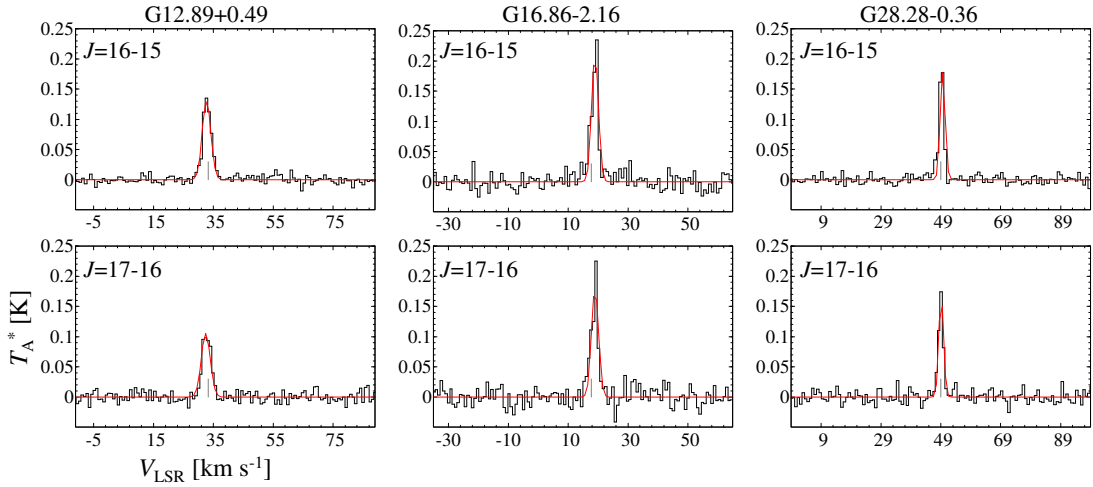


Figure 3. Spectra of HC_5N at the 42–46 GHz band toward the three hot cores with the Nobeyama 45 m telescope. The red lines show the results of the Gaussian fitting, and the vertical lines indicate the systemic velocity of each source.

previous paragraph ($T_{\text{rot}} = 16 \pm 4$ K, $N = 7.5^{+0.8}_{-0.6} \times 10^{12}$ cm $^{-2}$). We use the results with the beam-size correction in the following sections, because the fitting results are better.

4. DISCUSSION

4.1. Comparisons of the rotational temperature of HC_5N

We compare the results in the high-mass star-forming regions with that in the cyanopolyne peak in Taurus Molecular Cloud-1 (TMC-1 CP, $d = 140$ pc), which is a well studied dark cloud and carbon-chain-species-rich source. The derived excitation temperature of HC_5N in TMC-1 CP is 6.5 ± 0.2 K (Taniguchi et al. 2016a). The rotational temperatures of HC_5N in our three target high-mass star-forming regions except for G10.30-0.15, $\sim 13 - 20$ K, are significantly higher than the excitation temperature in the dark cloud TMC-1 CP.

The rotational temperature of HC_5N in the low-mass star-forming region L1527 ($d = 140$ pc) is known to be 14.7 ± 5.3 K (3σ , Sakai et al. 2009b). The rotational temperatures of HC_5N in our target high-mass star-forming regions are comparable with or slightly higher than that in L1527. L1527 is one of the WCCC sources, in which carbon-chain

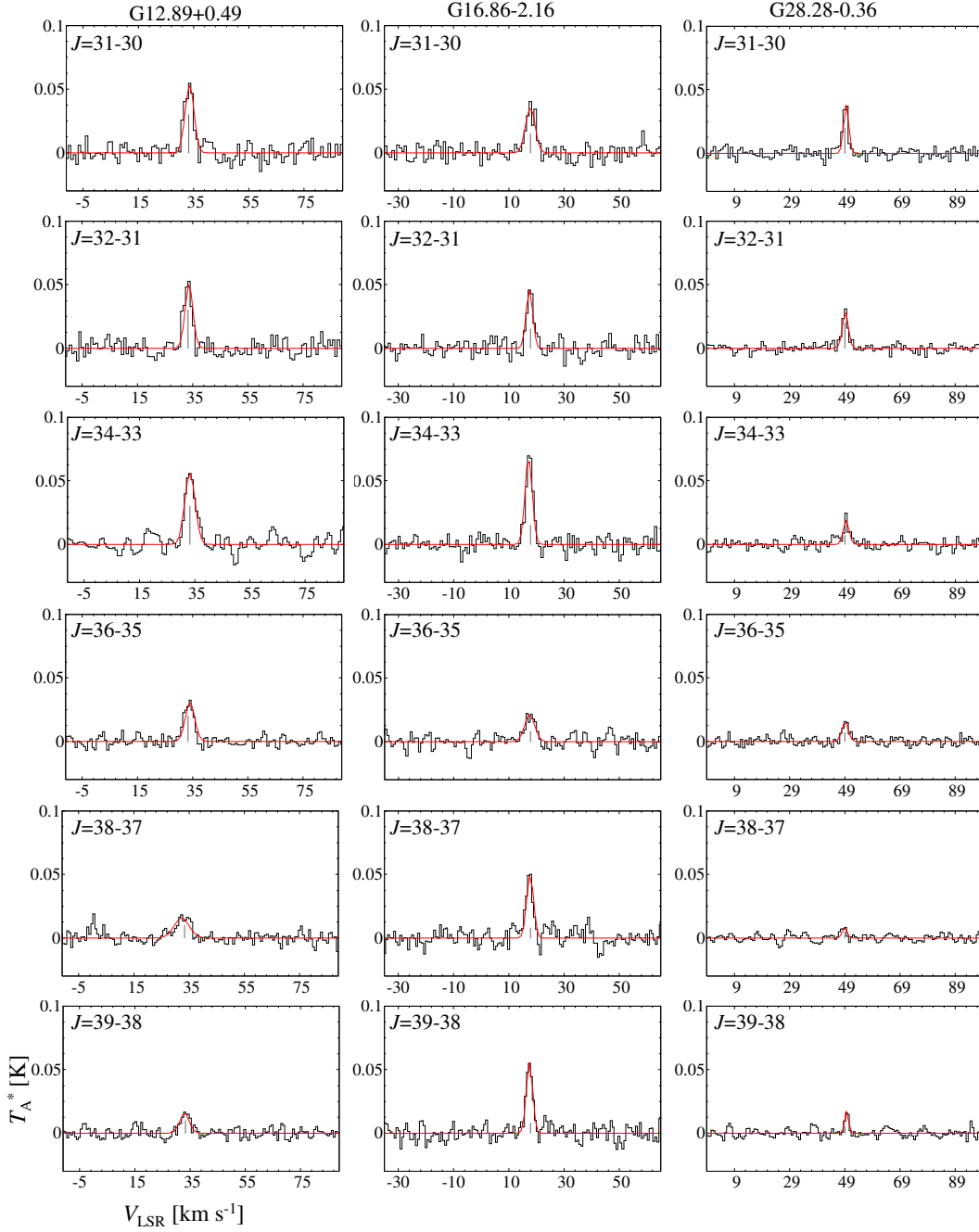


Figure 4. Spectra of HC₅N at the 82–103 GHz band toward the three hot cores with the Nobeyama 45 m telescope. The red lines show the results of the Gaussian fitting, and the vertical lines indicate the systemic velocity of each source.

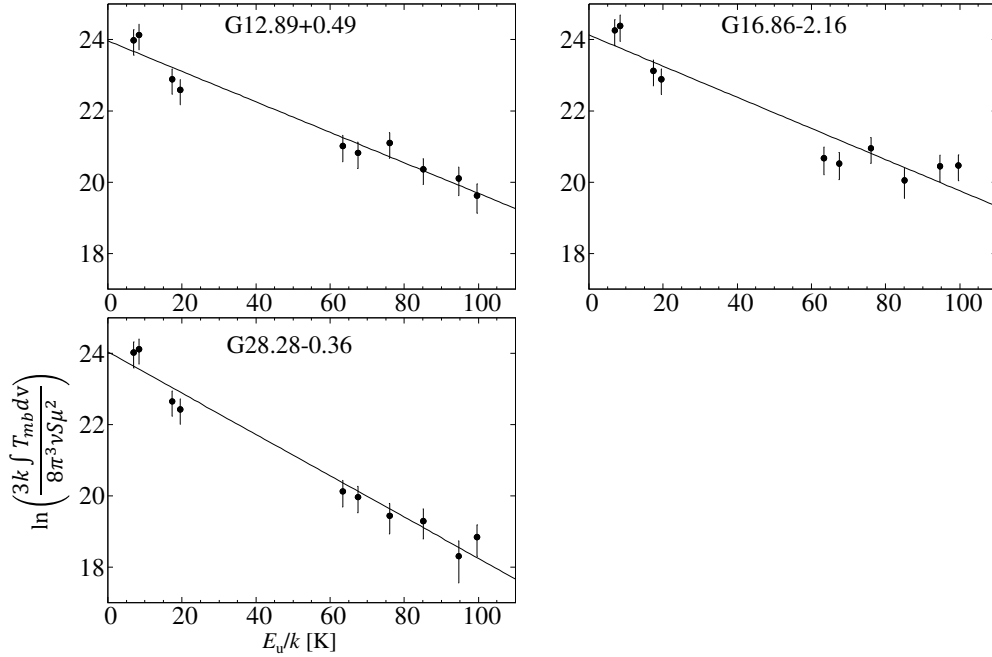


Figure 5. Rotational diagram of HC₅N toward the three sources with the filling factor of unity. The error bars show one standard deviation.

species are formed in the warm gas around the protostar with the temperature of $\sim 20 - 30$ K (Sakai & Yamamoto 2013). Therefore, HC₅N seems to exist in the warm gas in our target high-mass star-forming regions.

The detection of the emission lines with the high excitation energies also allows us to confirm the warm components of HC₅N by itself. The detected emission lines of HC₅N with the high-excitation energies ($E_u/k \sim 90 - 100$ K) should not come from the cold environments with the gas kinetic temperature of 10 K. We assume that the column density of HC₅N is comparable with that in TMC-1 CP ($N(\text{HC}_5\text{N}) = (6.2 \pm 0.3) \times 10^{13} \text{ cm}^{-2}$, Taniguchi et al. 2016a) and the rotational temperature is a typical gas kinetic temperature in cold dark cloud (10 K). The peak intensities of the $J = 38 - 37$ and $39 - 38$ lines are calculated to be 0.8 mK in T_A^* , even though the column density of the particular carbon-chain-rich source is considered. Thus, the detection of the emission lines of HC₅N with the energies of $\sim 90 - 100$

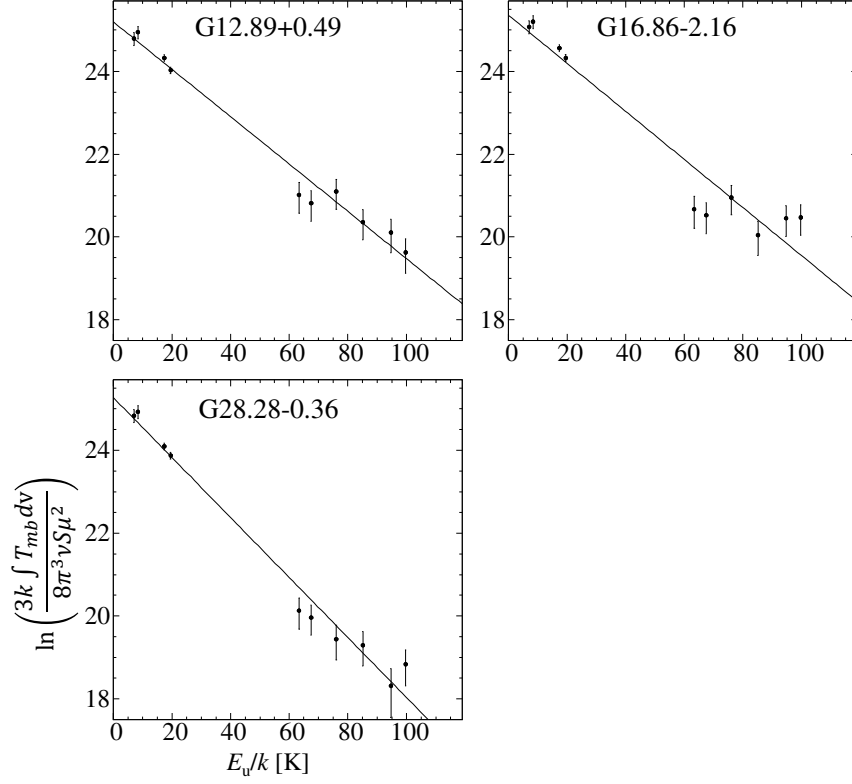


Figure 6. Rotational diagram of HC_5N toward the three sources with the beam-size correction. The error bars show one standard deviation.

K implies that HC_5N exists in the warm gas. There is a possibility that the emission lines with the energies of < 20 K come from not only the warm gas but also the cold gas. In that case, the derived rotational temperatures will be the lower limits due to the mixing of the warm gas and the cold gas in the single-dish beams. To summarize, we can conclude that HC_5N exists in the warm gas within $0.07\text{--}0.1$ pc radii around the massive young stellar objects.

Table 5. The rotational temperatures and column densities of HC₅N in the four sources

Source	filling factor = 1		With beam-size correction	
	T_{rot} (K)	N ($\times 10^{12}$ cm $^{-2}$)	T_{rot} (K)	N ($\times 10^{12}$ cm $^{-2}$)
G10.30-0.15	$21 \pm 11^{\text{a}}$	$8.5^{+2.0}_{-1.7}$	$16 \pm 4^{\text{a}}$	$7.5^{+0.8}_{-0.6}$
G12.89+0.49	23^{+7}_{-5}	$9.4^{+1.8}_{-2.0}$	18 ± 2	$23.9^{+1.5}_{-1.7}$
G16.86-2.16	23^{+7}_{-4}	11 ± 2	17 ± 2	$27.8^{+1.6}_{-2.0}$
G28.28-0.36	17^{+4}_{-3}	$7.5^{+1.9}_{-2.1}$	$13.8^{+1.5}_{-1.1}$	$20.5^{+2.0}_{-0.5}$

NOTE—The errors represent one standard deviation.

^aThe value is the average rotational temperature of the three sources except for G10.30-0.15. The error originates from those of the rotational temperatures in the three sources.

4.2. Possibility of chemical differentiation in the high-mass star-forming cores

4.2.1. $N(\text{HC}_5\text{N})/W(\text{CH}_3\text{OH})$ ratios in the four high-mass star-forming regions

We investigate the relationship between HC₅N and CH₃OH in the high-mass star-forming cores. CH₃OH is one of the representative hot core tracers and COMs, and its origin is considered to be different from carbon-chain molecules. Figure 7 shows the comparison of the ratios between $N(\text{HC}_5\text{N})$ the column density of HC₅N and $W(\text{CH}_3\text{OH})$ the integrated intensity of the thermal CH₃OH emission line summarized in Table 3. We cannot derive the excitation temperature and column density of CH₃OH due to the detection of only single line with low-excitation energy ($E_{\text{u}} < 50$ K). The other detected lines with high-excitation energies in G12.89+0.49 could possibly be masers (Müller et al. 2004). Therefore, we cannot use these lines to derive the excitation temperatures.

Since the column density of HC₅N in G10.30-0.15 was derived using its average rotational temperature of the other three high-mass star-forming regions, we do not discuss the result of G10.30-0.15 in detail due to its large uncertainty. We can divide three high-mass star-forming regions into two groups; G28.28-0.36 shows the largest $N(\text{HC}_5\text{N})/W(\text{CH}_3\text{OH})$ ratio of $> 8.0 \times 10^{14}$ in units of (K km s $^{-1}$) $^{-1}$ cm $^{-2}$, while those of G12.89+0.49 and G16.86-2.16 are only $(1.9 \pm 0.3) \times 10^{13}$ and $(2.6 \pm 0.5) \times 10^{13}$, respectively. The ratio in G28.28-0.36 is significantly larger than those in G12.89+0.49 and G16.86-2.16 by one order of magnitude, even though there is a possibility that the chemical and physical structures in the beams cause the observed large difference. The $N(\text{HC}_5\text{N})$ values are almost comparable among the three sources. Therefore, the differences in the $N(\text{HC}_5\text{N})/W(\text{CH}_3\text{OH})$ ratio come from the $W(\text{CH}_3\text{OH})$ values.

The integrated intensity is proportional to both the column density and the rotational temperature. When we assume the same $N(\text{HC}_5\text{N})/N(\text{CH}_3\text{OH})$ ratios in all of the three sources, the differences in the $N(\text{HC}_5\text{N})/W(\text{CH}_3\text{OH})$ ratios depend on only the rotational temperature of CH₃OH. If the rotational temperature of CH₃OH in G28.28-0.36 is the typical value in hot cores (100–250 K, Bisschop et al. 2007), the large difference in the integrated intensities of CH₃OH by an order of magnitude (e.g., for the case of G28.28-0.36 and G16.86-2.16) cannot be explained given any rotational temperature assumed in G16.86-2.16. Alternatively, if the rotational temperatures of CH₃OH in G12.89+0.49 and G16.86-2.16 are 100–250 K, G28.28-0.36 will have an unlikely high rotational temperature of CH₃OH, 1200–2600 K. Thus, the differences in the $N(\text{HC}_5\text{N})/W(\text{CH}_3\text{OH})$ ratio among the three sources cannot be explained only by changes in the rotational temperature of CH₃OH, but the column density of CH₃OH in G28.28-0.36 should be lower than those in G12.89+0.49 and G16.86-2.16. In summary, the observed variation in the $N(\text{HC}_5\text{N})/W(\text{CH}_3\text{OH})$ ratio reflects the chemical differentiation in the single-dish beams.

4.2.2. Fractional abundances of HC₅N in the four high-mass star-forming regions

We also derived the fractional abundances of HC₅N defined as $X(\text{HC}_5\text{N}) = N(\text{HC}_5\text{N})/N(\text{H}_2)$ toward the four sources. We calculated the column densities of H₂ from the SCUBA, installed on the James Clerk Maxwell Telescope, 850 μm continuum data using the following formula (Kauffmann 2005);

$$N(\text{H}_2) = 2.02 \times 10^{20} \text{cm}^{-2} \left(e^{1.439(\lambda/\text{mm})^{-1}(T/10\text{K})^{-1}} - 1 \right) \left(\frac{\kappa_{\nu}}{0.01 \text{cm}^2 \text{g}^{-1}} \right)^{-1} \left(\frac{S_{\nu}^{\text{beam}}}{\text{mJy beam}^{-1}} \right) \left(\frac{\theta_{\text{HPBW}}}{10 \text{arcsec}} \right)^{-2} \left(\frac{\lambda}{\text{mm}} \right)^3. \quad (2)$$

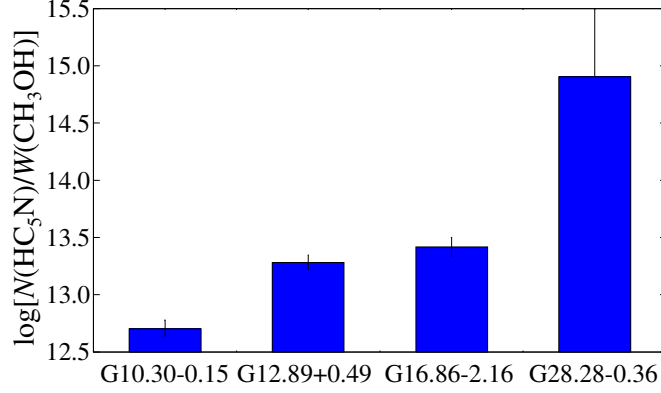


Figure 7. Ratios of $N(\text{HC}_5\text{N})/W(\text{CH}_3\text{OH})$ [$(\text{K km s}^{-1})^{-1} \text{ cm}^{-2}$] in the four high-mass star-forming regions. The error bars show the standard deviation. The value of $W(\text{CH}_3\text{OH})$ in G28.28-0.36 is the 4σ upper limit.

The continuum data were obtained from the Canadian Astronomy Data Center, JCMT Science Archive⁶. We used the continuum fluxes (S_ν^{beam}) toward the observed positions and the beam size ($18''$) as summarized in Table 6⁷. We used $0.0182 \text{ cm}^2 \text{ g}^{-1}$ for κ_ν (Kauffmann 2005), and $18''$ for θ_{HPBW} . T is the dust temperature obtained by SED fitting (Purcell et al. 2009), as summarized in Table 6. In G28.28-0.36, the dust temperature was not derived, and we used the average value of 58 K, determined from 65 good fits (Purcell et al. 2009). Table 6 summarizes the column densities of molecular hydrogen $N(\text{H}_2)$ and the $X(\text{HC}_5\text{N})$ values. The errors of $N(\text{H}_2)$ are derived assuming that uncertainty of the dust temperatures is 20 K.

Figure 8 shows the comparison of the $X(\text{HC}_5\text{N})$ values among the four sources. The $X(\text{HC}_5\text{N})$ values show the same tendency as the $N(\text{HC}_5\text{N})/W(\text{CH}_3\text{OH})$ ratios. G28.28-0.36 shows the largest $X(\text{HC}_5\text{N})$ value ($4.2_{-2.0}^{+2.6} \times 10^{-9}$) in the four sources, and G12.89+0.49 and G16.86-2.16 show the similar values, which is smaller than that in G28.28-0.36. As mentioned before, the column density of HC_5N in G10.30-0.15 was derived using the average rotational temperature of the three sources, and so we do not discuss in detail.

⁶ <http://www.cadc-ccda.hia-ihp.nrc-cnrc.gc.ca/en/jcmt/>

⁷ Proposal IDs are m05ai02 for G10.30-0.15, m03bc05 for G12.89+0.49, and m00au01 for G16.86-2.16 and G28.28-0.36, respectively.

Table 6. The values of 850 μm continuum flux, dust temperature, $N(\text{H}_2)$, and $X(\text{HC}_5\text{N})$ in the four hot cores

Source	850 μm flux (Jy beam $^{-1}$)	T^{a} (K)	$N(\text{H}_2)^{\text{b}}$ ($\times 10^{22}$ cm $^{-2}$)	$X(\text{HC}_5\text{N})$ ($\times 10^{-10}$)
G10.30-0.15	4.1	71	$1.2^{+0.7}_{-0.3}$	$6.3^{+3.2}_{-2.6}$
G12.89+0.49	5.8	54	$2.4^{+2.5}_{-0.8}$	$9.9^{+6.1}_{-5.4}$
G16.86-2.16	5.8	70	$1.7^{+1.0}_{-0.5}$	16 ± 7
G28.28-0.36	1.3	58 ^c	$0.49^{+0.42}_{-0.16}$	42^{+26}_{-20}

NOTE—The errors represent the standard deviation.

^aTaken from online material of Purcell et al. (2009).

^bThe errors were derived from the uncertainties of the dust temperatures of 20 K.

^cThe average value derived from 65 good fits (Purcell et al. 2009).

Both Figures 7 and 8 imply a possible signature of chemical differentiation among the high-mass star-forming cores, although we selected only four biased samples associated with HC_5N emission and the 6.7 GHz methanol masers. We cannot exclude a possibility of the chemical and physical structures in the beam, and one possible explanation for such chemical differentiation is the different beam filling factor of hot core regions (Hatchell et al. 1998). Observations to reveal the spatial distributions of carbon-chain molecules and COMs with the interferometry are essential for revealing the origin of the chemical differentiation.

The fractional abundance of HC_5N in L1527 was derived to be $\sim 2 \times 10^{-10}$ ($N(\text{HC}_5\text{N}) = (6.8 \pm 1.4) \times 10^{12}$ cm $^{-2}$ and $N(\text{H}_2) = 2.8 \times 10^{22}$ cm $^{-2}$ were derived by Sakai et al. (2009b) and Jørgensen et al. (2002), respectively). Even though there are uncertainties in column densities of H_2 and HC_5N due to assumed parameters (e.g. temperature, dust opacity, source size), the derive fractional abundances of HC_5N in the three high-mass star-forming regions (except for G10.30-0.15) are comparable to or slightly higher than that in L1527 by a factor of 5–20. Such high HC_5N abundances in our target sources suggest that the warm gas around these massive young stellar objects is rich in HC_5N . Moreover, the high HC_5N abundances would suggest efficient formation mechanisms of carbon chains in these high-mass star-forming regions (Aikawa et al. (2008) and Hassel et al. (2008) for WCCC and Chapman et al. (2009) for hot core).

5. CONCLUSIONS

We carried out line survey observations at the 26–30 GHz band toward the four high-mass star-forming regions containing hot cores, G10.30-0.15, G12.89+0.49, G16.86-2.16, and G28.28-0.36, with the Robert C. Byrd Green Bank Telescope. We have detected HC_5N from all of the sources, and HC_7N from the three sources except for G10.30-0.15. The detection of HC_7N means that these high-mass star-forming regions contain plenty of long cyanopolyynes compared to typical star-forming regions.

We also conducted observations of HC_5N at the 42–46 GHz and 82–103 GHz bands toward the three high-mass star-forming regions, G12.89+0.49, G16.86-2.16, and G28.28-0.36, with the Nobeyama 45 m radio telescope. We have detected the rotational lines of HC_5N with the high excitation energies ($E_{\text{u}}/k \sim 63 - 100$ K), which are hardly excited in the cold dark clouds. We conducted the rotational diagram analysis, combining the GBT data with the Nobeyama data. The rotational temperatures of HC_5N in the three high-mass star-forming regions are derived to be $\sim 13 - 20$ K. The detection of the lines with the high excitation energies and the derived rotational temperatures indicate that HC_5N exists in the warm gas within 0.07–0.1 pc radii around the massive young stellar objects. The derived column densities of HC_5N in the three sources are ($\sim 2.0 - 2.8$) $\times 10^{13}$ cm $^{-2}$.

We compare the ratios between the column density of HC_5N , $N(\text{HC}_5\text{N})$, and the integrated intensity of the thermal CH_3OH emission line, $W(\text{CH}_3\text{OH})$ among the three high-mass star-forming regions. We found a possibility of the chemical differentiation in the three high-mass star-forming regions; G28.28-0.36 shows the largest $N(\text{HC}_5\text{N})/W(\text{CH}_3\text{OH})$ ratio of $> 8.0 \times 10^{14}$ in units of (K km s $^{-1}$) $^{-1}$ cm $^{-2}$, while G12.89+0.49 and G16.86-2.16 show the smaller values

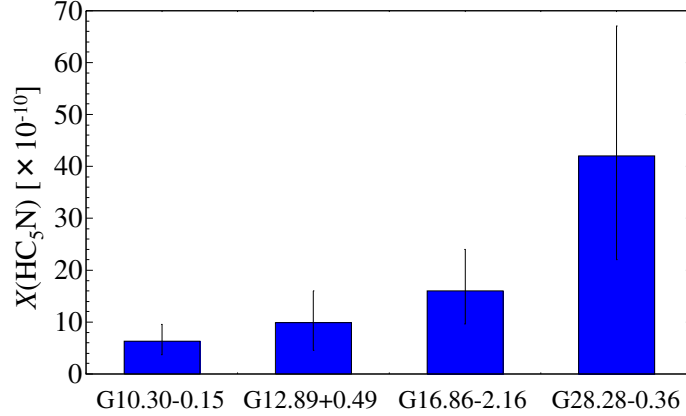


Figure 8. Fractional abundances of HC_5N , $X(\text{HC}_5\text{N})$, in the four high-mass star-forming regions. The error bars show the standard deviation.

($\sim 2 \times 10^{13}$). Such chemical differentiation may originate from the complex chemical and physical structures in the beam.

We deeply appreciate the anonymous referee for constructive suggestions, which are very useful to develop our discussion. We would like to express our great thanks to the staff members of the National Radio Astronomy Observatory. The National Radio Astronomy Observatory is a facility of the National Science Foundation operated under cooperative agreement by Associated Universities, Inc. K. T. deeply appreciates Dr. Nichol Cunningham (NRAO) for her kind help to prepare and carry out observations. We would like to express our thanks to the staff members of the Nobeyama Radio Observatory. The Nobeyama Radio Observatory is a branch of the National Astronomical Observatory of Japan, National Institutes of Natural Sciences.

Facilities: Robert C. Byrd Green Bank Telescope, Nobeyama 45 m radio telescope

Software: GBTIDL, Java Newstar

REFERENCES

- Aikawa, Y., Wakelman, V., Garrod, R. T., & Herbst, E. 2008, *ApJ*, 674, 993
- Alexander, A. J., Kroto, H. W., & Walton, D. R. M. 1976, *JMoSp*, 62, 175
- Bergin, E. A., Snell, R. L., & Goldsmith, P. F. 1996, *ApJ*, 460, 343
- Bisschop, S. E., Jørgensen, J. K., van Dishoeck, E. F., & de Wachter, E. B. M. 2007, *A&A*, 465, 913
- Chapman, J. F., Millar, T. J., Wardle, M., Burton, M. G., & Walsh, A. J. 2009, *MNRAS*, 394, 221
- Cordiner, M. A., Charnley, S. B., Wirström, E. S., & Smith, R. G. 2012, *ApJ*, 744, 131
- Cyganowski, C. J., Whitney, B. A., Holden, E., et al. 2008, *AJ*, 136, 2391
- Feng, S., Beuther, H., Henning, Th., et al. 2015, *A&A*, 581, A71
- Friesen, R. K., Medeiros, L., Schnee, S., et al. 2013, *MNRAS*, 436, 1513
- Garrod, R. T., & Herbst, E. 2006, *A&A*, 457, 927
- Goddi, C., Greenhill, L. J., Humphreys, E. M. L., Chandler, C. J., & Matthews, L. D. 2011, *ApJL*, 739, L13
- Goldsmith, P. F., & Langer, W. D. 1999, *ApJ*, 517, 209
- Green, C. -E., Green, J. A., Burton, M. G., et al. 2014, *MNRAS*, 443, 2252
- Hassel, G. E., Herbst, E., & Garrod, R. T. 2008, *ApJ*, 681, 1385
- Hatchell, J., Thompson, M. A., Millar, T. J., & MacDonald, G. H. 1998, *A&AS*, 133, 29
- Herbst, E., & van Dishoeck, E. F. 2009, *ARA&A*, 47, 427
- Hirota, T., M. Ohishi, & Yamamoto, S. 2009, *ApJ*, 699, 585
- Jørgensen, J. K., Schöier, F. L., & van Dishoeck, E. F. 2002, *A&A*, 389, 908
- Kamazaki, T., Okumura, S. K., Chikada, Y., et al. 2012, *PASJ*, 64, 29
- Kauffmann, J. 2005, Column Densities and Masses from Dust Emission,
<http://youngstars.nbi.dk/jeskj/AstroSpectra/kauffmann05.pdf>
- Li, F. C., Xu, Y., Wu, Y. W., et al. 2016, *AJ*, 152, 92
- Müller, H. S. P., Menten, K. M., & Mäder, H. 2004, *A&A*, 428, 1019
- Müller, H. S. P., Schlöder, F., Stutzki, J., & Winnewisser, G. 2005, *JMoSt*, 742, 215
- Nakajima, T., Kimura, K., Nishimura, A., et al. 2013, *PASP*, 125, 252
- Nakamura, F., Ogawa, H., Yonekura, Y., et al. 2015, *PASJ*, 67, 117
- Purcell, C. R., Balasubramanyam, R., Burton, M. G., et al. 2006, *MNRAS*, 367, 553
- Purcell, C. R., Longmore, S. N., Burton, M. G., et al. 2009, *MNRAS*, 394, 323
- Reid, M. J., Menten, K. M., Brunthaler, A., et al. 2014, *ApJ*, 783, 130
- Sakai, N., Sakai, T., Hirota, T., & Yamamoto, S. 2008, *ApJ*, 672, 371
- Sakai, N., Sakai, T., Hirota, T., Burton, M., & Yamamoto, S. 2009a, *ApJ*, 697, 769
- Sakai, N., Sakai, T., Hirota, T., & Yamamoto, S. 2009b, *ApJ*, 702, 1025
- Sakai, N., Sakai, T., Hirota, T., & Yamamoto, S. 2010, *ApJ*, 722, 1633
- Sakai, N., & Yamamoto, S. 2013, *ChRv*, 113, 8981
- Suzuki, H., Yamamoto, S., Ohishi, M., et al. 1992, *ApJ*, 392, 551
- Taniguchi, K., Ozeki, H., Saito, M., et al. 2016a, *ApJ*, 817, 147
- Taniguchi, K., Saito, M., & Ozeki, H. 2016b, *ApJ*, 830, 106
- Thompson, M. A., Hatchell, J., Walsh, A. J., Macdonald, G. H., & Millar, T. J. 2006, *A&A*, 453, 1003
- Walsh, A. J., Macdonald, G. H., Alvey, N. D. S., Burton, M. G., & Lee, J. 2003, *A&A*, 410, 597